Supplementary Materials document includes:

- Note 1. Remapping of the South Florida Water Management District (SFWMD) Land Cover map.
- Figure S1. Comparison between during-event backscatter deviations from linear models to Mean Absolute Errors (MAE) for EDEN water gauges.
- Note 2. Evaluation of Hurricane Irma's wind impact on during-event backscatter values.
- Figure S2. Water gauges with combined positive and negative linear σ°-d_w relationships.
- Figure S3. The locations of the water gauges with combined positive and negative σ°-d_w relationships shown in Figure S2.
- Figure S4. Normalized Difference Backscatter Index (NDBI) for the during-event (September 10) and five post-event SAR dates.
- Table S1. SWDI detection parameters and validation metrics with a threshold of 12 cm (n_{th} = 3) using the combined criteria of NDBI > n_{th} or NDBI < -n_{th}.
- Table S2. SWDI detection parameters and validation metrics with a threshold of 8 cm (n_{th} = 2).
- Table S3. SWDI classification threshold parameters and validation metrics using C-VH data.
- Table S4. SWDI validation metrics using C-VH data based on the optimal set of thresholds: n_{SWDI} = 20%, and $n_{Non\text{-}SWDI}$ = 10%.
- Figure S5. C-VH σ°-d_w scatter plot for EDEN water gauge '3B-SE' characterized by a negative linear relationship.

Note 1. Remapping of the South Florida Water Management District (SFWMD) Land Cover map.

The Land cover map of the study area in the Everglades, Figure 2, was derived from the South Florida Water Management District (SFWMD) Land Cover Use map for the period of 2014 - 2016, which was the most recent land cover map for the entire Everglades (https://geo-sfwmd.hub.arcgis.com/datasets/sfwmd::sfwmd-land-cover-land-use-2014-2016/about). We remapped the land cover map into three classes: 'Herbaceous', 'Trees embedded in herbaceous matrix', 'Others', by

merging different Level 2 classes provided in the original dataset. 'Herbaceous' class includes 'Vegetated Non-Forested Wetlands' and 'Mixed Rangeland' land covers; 'Trees embedded in herbaceous matrix' class includes '4400 Tree Plantations', 'Tree Crops', 'Upland Coniferous Forests', 'Upland Hardwood Forests', 'Upland Mixed Forests', 'Wetland Coniferous Forests', 'Wetland Forested Mixed', 'Wetland Hardwood Forests'; 'Others' includes the rest of land covers, which only occupy a relatively small portion of the entire area.

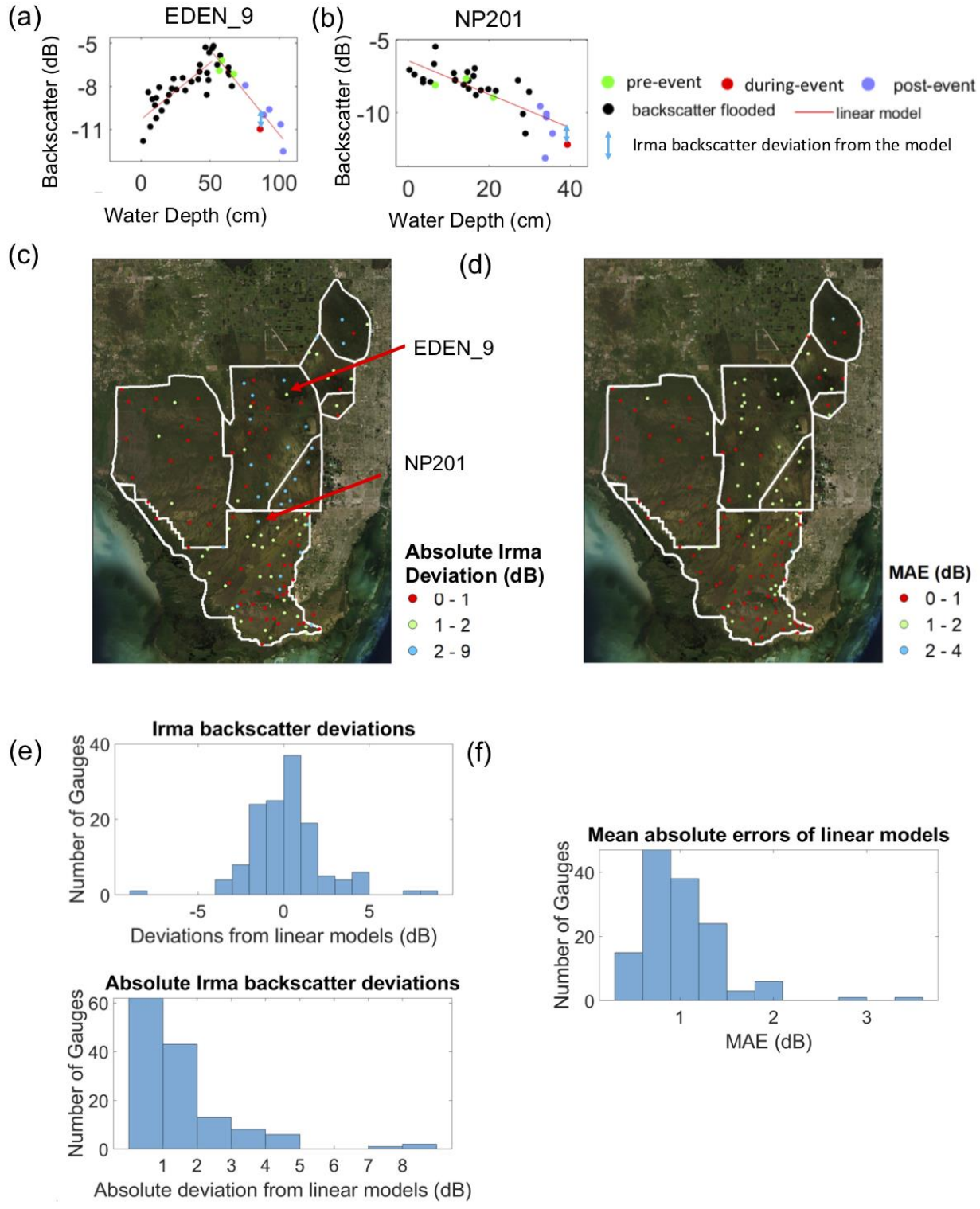

Figure S1. Comparison between during-event backscatter deviations from linear models to Mean Absolute Errors (MAE) for EDEN water gauges. (**a, b**) two selected pixels from Figure 4 (gauges 'EDEN_9' and 'NP201') in the

manuscript illustrating during-event (Irma acquisition) backscatter deviations from linear models represented by light blue arrows. The other symbols share the same legend with Figure 4. (**c, d**) Spatial distribution of Irma backscatter deviations and MAE at water gauge locations, respectively. The locations of the two selected gauges were labelled in (c). (**e**) Histogram of Hurricane Irma backscatter deviations and their absolute values for 135 selected water gauges. (**f**) Histogram of MAE for the gauges.

Note 2. Evaluation of Hurricane Irma's wind impact on during-event backscatter values.

We selected 135 gauges and classified them into positive, combined positive-negative, and negative backscatter-water depth linear relationships using the methodology provided by Zhang et al. [25] and calculated for each gauge the during-event backscatter's deviation from the linear model (blue vertical arrows in Figure S1a, S1b), and the mean absolute deviation (MAE), i.e., the average of absolute deviation of all SAR acquisitions used for the linear model. We compared Irma deviations with MAE to evaluate if Hurricane Irma caused notable changes in backscatter or not.

We mapped the distribution of the 135 used water gauges distributed throughout the study area with Irma deviations and MAE values, respectively (Figure S1c, S1d), and the two variables were at similar levels (most of them < 2dB). Also, the movement of eye of Hurricane Irma on September 10, 2017 (during-event date) was in the Gulf of Mexico, west of the Everglades. However, gauges at the west of the study area showed smaller Irma deviations than those in the east (Figure S1c), which further indicated that Irma's wind does not make significant impact on backscatter of vegetation.

Figure S1e shows the histogram of during-event backscatter deviation values (observed - model backscatter), which has a mean about 0 dB. It showed observed backscatter's deviations can be either positive or negative from linear model predictions (Figure S1e). Also, the histogram of absolute Irma deviations showed the majority of water gauges have deviations less than 2 dB, similar to the MAE

histogram (Figure S1e and f), that represent average absolute deviations for SAR data used for calculating the linear models.

To conclude, the assumption that water depth is the dominant factor determining backscatter values is valid for the during-event date and the wind's impact on backscatter is neglectable.

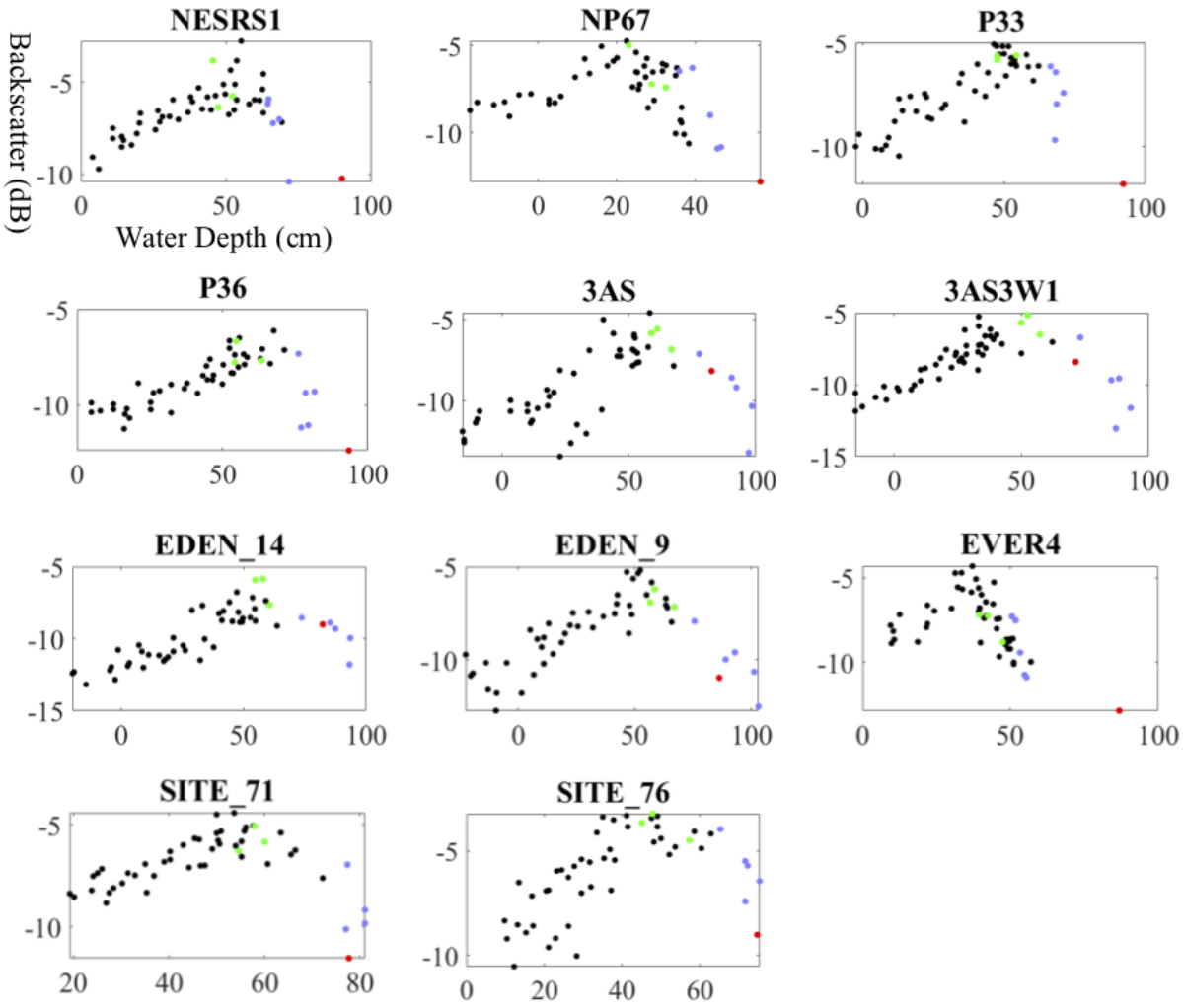

Figure S2. Water gauges with combined positive and negative linear σ°-d_w relationships. The x-axis denotes water depth (cm) and y-axis backscatter (dB) as indicated by the first sub-plot. Green, red, and blue dots denote pre-, during- and post-event observations, respectively. All scatter plots show the three selected pre-event observations are

located at the "hinge" area or along with the negative linear model, with water depth increases inducing backscatter decreases.

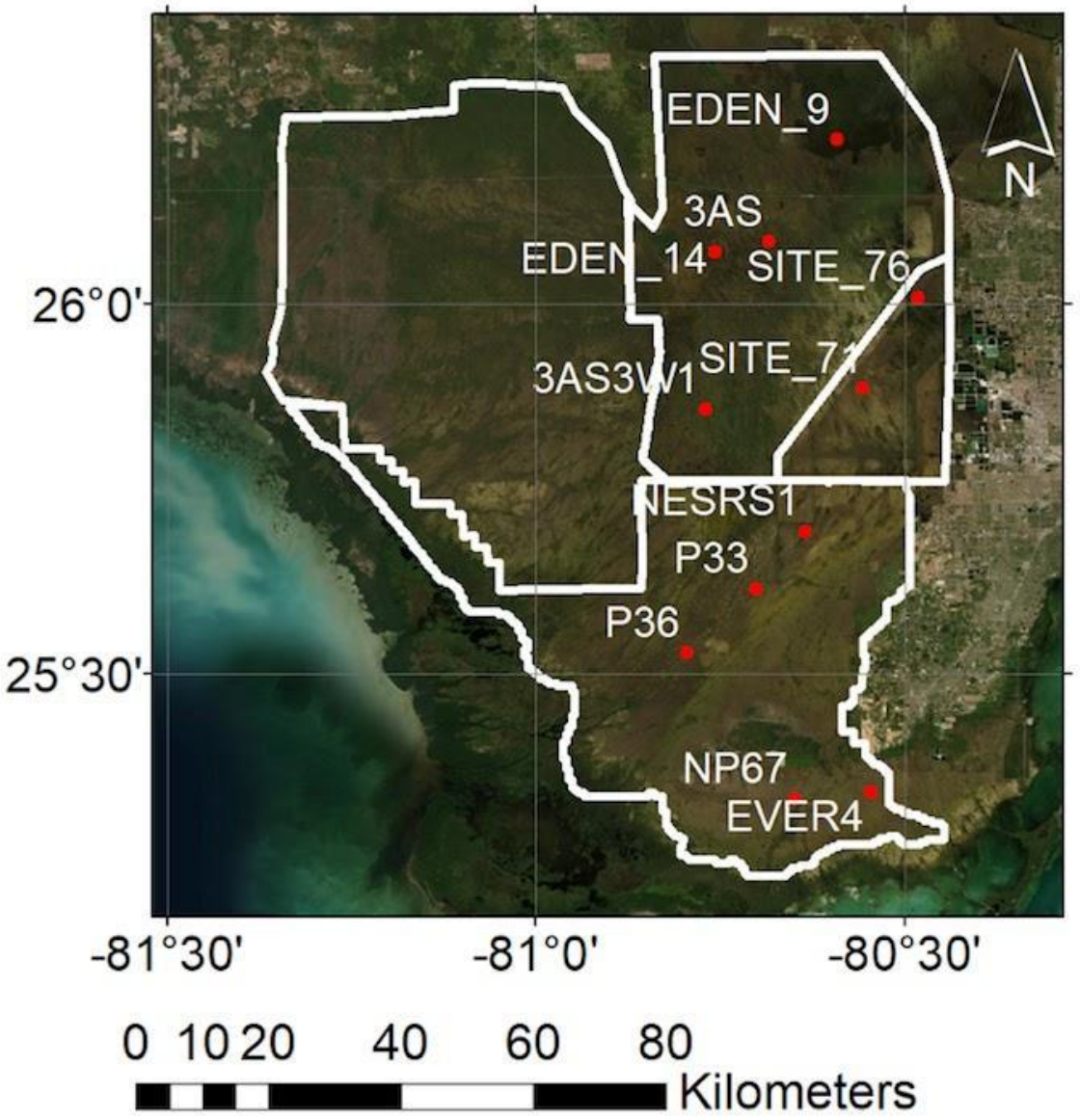

Figure S3. The locations of the water gauges with combined positive and negative σ°-d_w relationships shown in Figure S2.

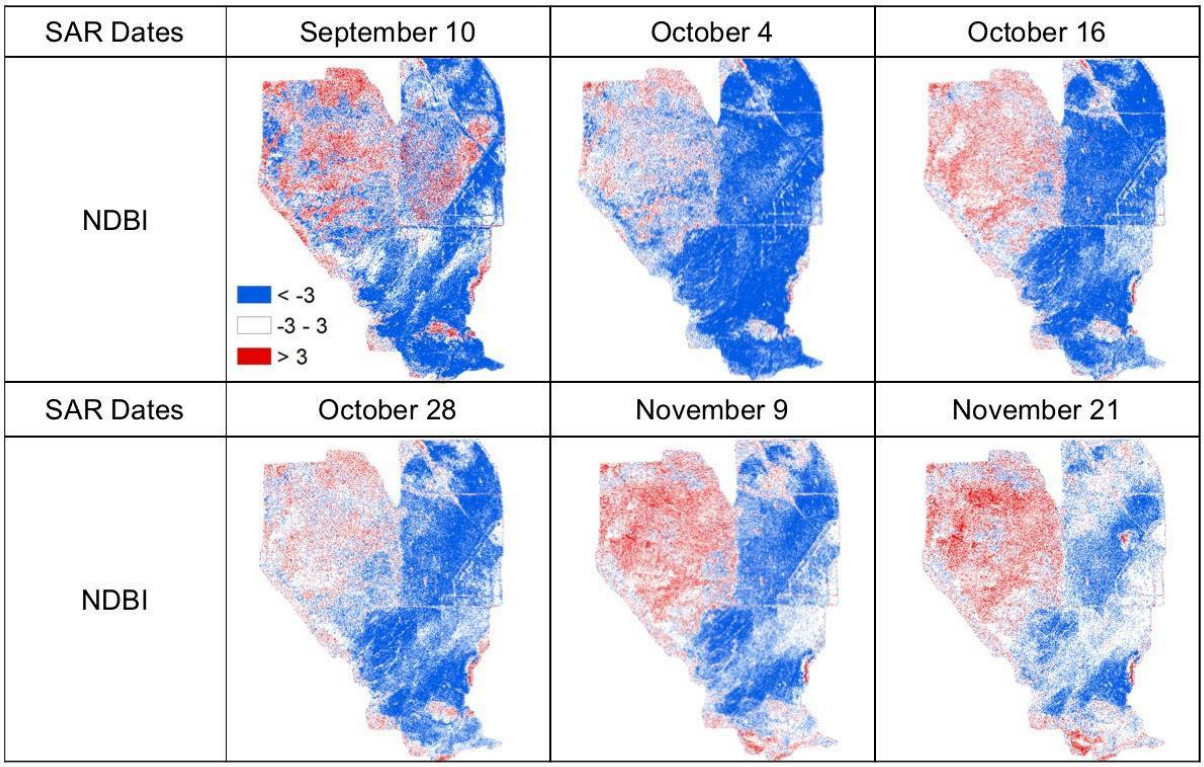

Figure S4. Normalized Difference Backscatter Index (NDBI) for the during-event (September 10) and five post-event SAR dates.

Table S1. SWDI detection parameters and validation metrics with a threshold of 12 cm (n_{th} = 3) using the combined criteria of NDBI > n_{th} or NDBI < -n_{th}.

n_{SWDI} (%)	$n_{Non\text{-}SWDI}$ (%)	Overall Accuracy	Kappa Coefficient	Average Uncertain Pixels Percentage
50	15	0.85	0.5	0.5
50	20	0.8	0.5	0.41
45	20	0.8	0.49	0.37
50	25	0.75	0.48	0.31
45	15	0.84	0.47	0.46
45	25	0.76	0.47	0.27
40	20	0.79	0.46	0.32
50	10	0.89	0.46	0.56
40	25	0.75	0.45	0.22
50	30	0.72	0.44	0.22
45	30	0.72	0.44	0.18
40	15	0.83	0.43	0.42

Table S2. SWDI detection parameters and validation metrics with a threshold of 8 cm (n_{th} = 2).

n_{SWDI} (%)	$n_{Non\text{-}SWDI}$ (%)	Overall Accuracy	Kappa Coefficient	Average Uncertain Pixels Percentage
50	10	0.83	0.57	0.32
45	10	0.84	0.57	0.29
40	10	0.84	0.57	0.27
35	10	0.84	0.56	0.24
30	10	0.84	0.55	0.2
25	10	0.84	0.54	0.17
45	15	0.8	0.52	0.23
50	15	0.79	0.52	0.25
40	15	0.8	0.52	0.2
35	15	0.8	0.52	0.17
20	10	0.83	0.51	0.12
30	15	0.81	0.51	0.14

Table S3. SWDI classification threshold parameters and validation metrics using C-VH data.

n_{SWDI} (%)	$n_{Non\text{-}SWDI}$ (%)	Overall Accuracy	Kappa Coefficient	Average Uncertain Pixels Percentage
15	10	0.62	0.32	0.07
10	10	0.63	0.32	0
20	10	0.61	0.31	0.12
25	10	0.6	0.3	0.15
15	15	0.59	0.29	0
30	10	0.58	0.29	0.18
20	15	0.58	0.28	0.05
35	10	0.57	0.27	0.21
25	15	0.57	0.27	0.08
20	20	0.56	0.26	0
30	15	0.56	0.25	0.11
40	10	0.56	0.25	0.23

Table S4. SWDI validation metrics using C-VH data based on the optimal set of thresholds: n_{SWDI} = 20%, and $n_{Non\text{-}SWDI}$ = 10%. Pixel percentages for 'True SWDI', 'False SWDI', 'False Non-SWDI', 'True Non-SWDI' were calculated based on the detected 'SWDI' and 'Non-SWDI' classes, without taking into account the 'Uncertain' class.

Date	True SWDI	False SWDI	False Non-SWDI	True Non-SWDI	Uncert. Pixels	OA	Kappa	SWDI		Non-SWDI	
								User	Producer	User	Producer
20170910	0.04	0	0.89	0.07	0.03	0.11	0	0.96	0.04	0.08	0.98
20171004	0.59	0.02	0.28	0.12	0.17	0.71	0.31	0.97	0.68	0.3	0.88
20171016	0.49	0.01	0.23	0.27	0.1	0.76	0.52	0.99	0.68	0.54	0.98
20171028	0.31	0	0.32	0.36	0.11	0.67	0.41	0.99	0.49	0.53	0.99
20171109	0.38	0	0.2	0.42	0.11	0.8	0.61	0.99	0.66	0.68	0.99
20171121	0.14	0.02	0.31	0.53	0.18	0.67	0.29	0.87	0.31	0.63	0.96

Table S5. Results of the sensitivity test using different pre-event water depth standard deviations.

Pre-event water depth standard deviation (cm)	SWDI detection threshold (cm) using n_{th} as 3	Overall Accuracy for SWDI detection
2	6	0.76
3	9	0.79
4	12	0.81
5	15	0.80
6	18	0.75

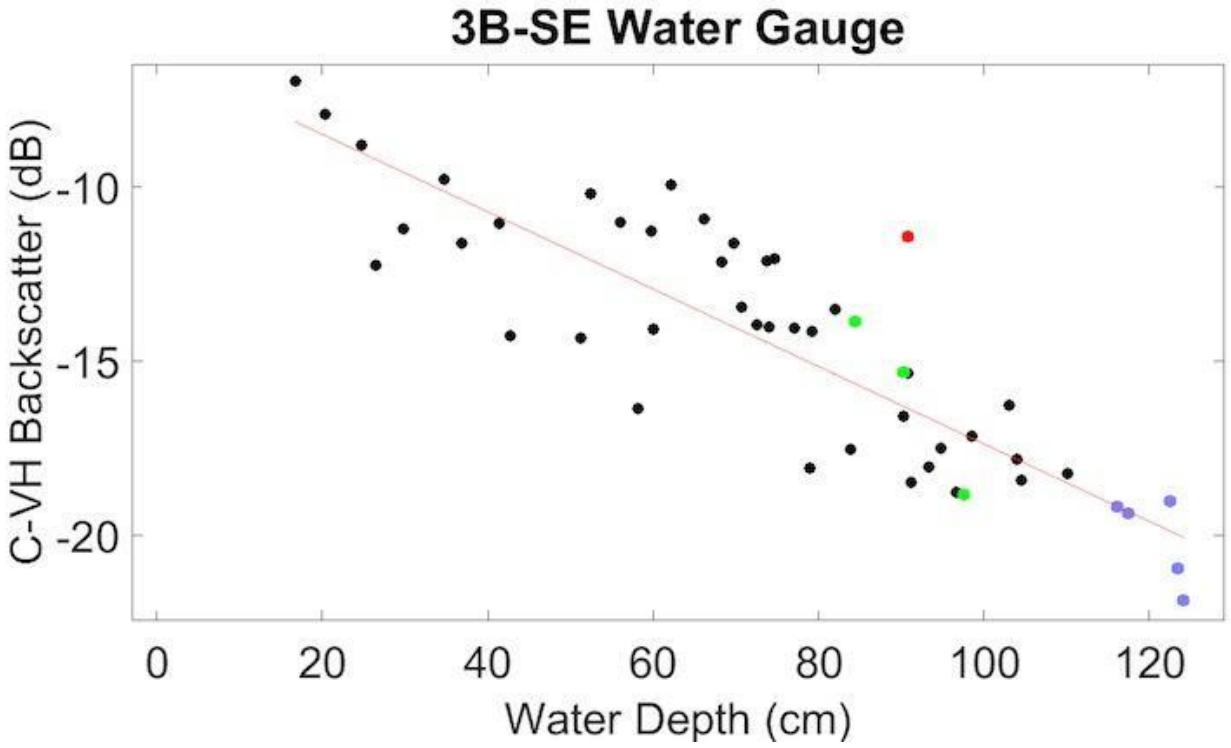

Figure S5. C-VH σ°-d_w scatter plot for EDEN water gauge '3B-SE' characterized by a negative linear relationship. Black dots represent the 2-year observations from September 2016 to September 2018; green, red, and blue dots represent pre-, during-, and post-event observations, the same as Figure 4. During-event backscatter shows a significant positive deviation from the best-fitting linear model.